Hydration and Confinement Effects on Horse Heart Myoglobin Adsorption in Mesoporous TiO2
Peer-reviewed author version

1 **Hydration and Confinement Effects on Horse Heart Myoglobin Adsorption in**

2 **Mesoporous TiO₂**

3 Stefano Loreto[a], Zainab Hafideddine[bc], Bert Cuypers[b], Robert Carleer[d], Sabine Van Doorslaer[b]

4 and Vera Meynen[a*]

5 [a] Laboratory for Adsorption and Catalysis (LADCA), Department of Chemistry, University of

6 Antwerp, Universiteitplein 1, 2610 Wilrijk, Belgium.

7 [b] Laboratory of Biophysics and Biomedical Physics (BIMEF), Department of Physics, University

8 of Antwerp, Universiteitplein 1, 2610 Wilrijk, Belgium

9 [c] Laboratory of Proteinchemistry, Proteomics and Epigenetic Signaling (PPES), Department of

10 Biomedical Sciences, University of Antwerp, Universiteitplein 1, 2610 Wilrijk, Belgium

11 [d] Laboratory for Applied and Analytical Chemistry (TANC), Institute for Material Research

12 (IMO), University of Hasselt, Agoralaan, 3590 Diepenbeek, Belgium

13 *Corresponding author email: vera.meynen@uantwerpen.be

Abstract

15 Despite the intensive research on protein adsorption in mesoporous materials, the effect of

16 (de)hydration and confinement on the adsorbed protein's stability and activity is poorly

17 understood. In this paper, we study the effect of differences in structural features (pore size)

18 and drying time on the adsorption and structural stability of horse heart myoglobin (hhMb)

19 on mesoporous titanium dioxide. Infrared spectroscopy (DRIFT) and thermal analysis (TGA)

20 coupled to a quadrupole mass spectrometer (TGA-MS) were used to evaluate the impact of

21 the confinement in different pores and hydration on the myoglobin secondary structure.

Electron paramagnetic spectroscopy (EPR) was applied to identify the changes in the heme and its close surrounding. The peroxidase-like activity of myoglobin toward 2,2'-azino-bis(3-ethylbenzthiazoline-6-sulfonic acid) (ABTS) in the presence of hydrogen peroxide allowed to detect changes in the protein activity after adsorption in pores with different sizes and drying for different periods of time. The results show a clear effect of the pore size and drying time on the secondary structure of hhMb, which is confirmed by differences induced in the catalytic activity of the adsorbed proteins. Therefore, we recommend to evaluate the effect of both hydration and confinement in future application involving biomolecule adsorption in porous matrices.

Introduction

Immobilization of proteins and enzymes (catalytic active proteins) in mesoporous material is a well-known strategy to improve their stability in different applications[1–3]. The protein stability is in this context defined as the protein ability to retain its native folded conformation upon adsorption in the mesoporous material. In 2001 Eggers and Valentine identified two main factors responsible for enhanced protein stability upon adsorption in a porous network: the space constriction and the water structure changes[4,5].

It is widely accepted that the reduced volume inside the pores stabilizes the native folded state of the proteins[6–8]. The degree of this stabilization is strongly dependent on the ratio between the protein dimension and the pore size[9]. In fact, the mobility and the 3-dimensional structure of the incorporated biomolecule depends on the number of contact points and strengths of interaction with the pore walls, and thus on the space availability inside the pores[1]. A recent work indicates that a 4-5 ratio between the pore size and the protein diameter is optimal if one wants full coverage of the inner surface in a reasonable time[10].

1	However, conflicting reports exist whether the pores should be much larger than the protein

2	dimensions or of similar size to achieve the highest protein stability upon adsorption. In

3	addition, divergent results have been reported on the effect of pore confinement on protein

4	activity. In fact, enhanced catalytic activity has been observed for myoglobin upon adsorption

5	in mesoporous silica (6 nm pores)[11] and mesoporous silica sheets (6 and 8 nm pores)[12]. On the

6	contrary, reduced activities have been observed for myoglobin[13] and cellulase[14] upon

7	adsorption in SBA-15 with different pore sizes.

8	On the other hand, very little is known about how (de)hydration influences the stability of

9	proteins confined in a porous network[15]. Nevertheless, this is of fundamental importance as

10	the total confinement effect on the protein stability may be dependent on changes of protein

11	hydration inside the pores[16,17]. Furthermore, it has been shown that the hydration and the

12	availability of water in the proximity of enzymes have a large effect on both their structure

13	and activity[18].

14	Zhang described it as follows, *"proteins are like fish in that they need water to survive, without*

15	*they lose vitality and become unable to carry out their functions"*[19]. Hence, any attempt toward

16	incorporation of proteins in a porous material should be carried out with attention for the

17	hydration of the biomolecule[20]. This assumption has been confirmed by Ravindra *et al.,* who

18	identified both hydration and space confinement as factors determining the stability of

19	proteins upon adsorption in mesoporous silica[21]. In addition, a recent study shows the

20	influence of hydration on the sidechains and backbone of ubiquitin immobilized in

21	mesoporous MCM materials[22].

Nevertheless, in the field of protein immobilization, with the exception of a few papers, the (de)hydration effect is mostly ignored and only the impact of the volume reduction has been considered.

Even though it has been reported that the magnitude of the confinement effect is strongly dependent on the structure of the pore network[9,23], the attention has mostly been focused on proteins incorporated in silica supports. This is a clear hiatus since much more promising mesoporous materials have been proposed as supports for protein incorporation in application like e.g. biosensors to avoid the limited electric properties of silica[24]. Titanium dioxide (titania) is one of the most used non-silica substrates for biomolecule incorporation[25–31]. The physicochemical properties of this semiconductor (e.g. charge transfer and photocatalytic activity) and its biomechanical stability make it a suitable substrate for innovative applications[32–34]. Moreover, our recently reported approach to tune the pore size of mesoporous TiO_2 with a narrow pore-size distribution[35] allows adsorption of proteins in a designed confined space.

Therefore, to obtain a deeper understanding on the impact of protein confinement in mesoporous titania, we describe in this paper the effect of confinement and (de)hydration on protein stability and activity after incorporation of horse heart myoglobin (hhMb) in mesoporous TiO_2 with pore size of 8 (MT8) and 17 nm (MT17). HhMb is a relatively small globin protein with a maximum diameter of ca 5 nm[36] containing a single iron protoporphyrin IX as the prosthetic group (heme) in a hydrophobic pocket[37]. Its protein fold consists of eight α-helices that are organized in a canonical 3-over-3 sandwich and that are labelled with letters A to H from the N- to the C-terminus. We chose hhMb as a test protein because of its high stability and solubility in water and its commercial availability.

The stability and activity of the hhMb upon adsorption and after different drying times are thoroughly studied using standard and advanced characterization tools. Specific attention is given to the changes in the structure of hhMb by using Infrared (DRIFT) spectroscopy in combination with thermal analysis (TGA) coupled to a quadrupole mass spectrometer (TGA-MS). In-depth information about the effect of (de)hydration and confinement on the heme center will be provided by electron paramagnetic resonance spectroscopy (EPR). Moreover, the chemical activity of the hhMb upon incorporation and its possible correlation with the pore size and drying time has been evaluated through its peroxidase activity toward 2,2'-azino-bis(3-ethylbenzthiazoline-6-sulfonic acid) (ABTS)[12].

We aim at clarifying the coinciding effect of structural properties (space confinement and/or surface chemistry) and (de)hydration on the protein stability and activity upon adsorption in a (designed) porous titania network. In addition, we intend to reveal the effect of the incorporation-induced structural rearrangements on the protein activity and relate it to the differences in (de)hydration and confinement.

Experimental

Materials

Myoglobin from equine heart (lyophilized powders, ≥90%, CAS: 100684-32-0), titanium (IV) butoxide (≥97%, CAS: 5593-70-4), acetic acid (≥99%, CAS: 64-19-7), nitric acid (70% v/v, CAS: 7697-37-2), sulfuric acid (95% v/v, CAS: 7664-93-9), HEPES buffer (≥95.5%, CAS: 7365-45-9), ethanol (≥99%, CAS: 64-17-5) and Poly(ethylene glycol)-*block*-poly(propylene glycol)-*block*-poly(ethylene glycol) (P123, CAS:9003-11-6) were purchased from Sigma Aldrich and used without further purifications.

Synthesis of Mesoporous TiO$_2$

The mesoporous substrates with different pore sizes were obtained by changing the inorganic acids added to the synthesis mixture as described in our recent publication[35]. Briefly, titanium butoxide was used as a precursor and dissolved in an aqueous acetic acid solution (20% v/v), then 4 g of P123 was added as template and HCl and H$_2$SO$_4$ were used to tune the pore size. After hydrothermal treatment at 120 $^{\circ}$C, the samples were collected, washed with distilled water, dried and calcined at 450 $^{\circ}$C in air for 4 h, the calcination temperature was reached with a heating rate of 1 $^{\circ}$C/min.

Immobilization of hhMb

In a typical experiment, 10 mg of mesoporous TiO$_2$ with pores of 8 (MT8) and 17 nm (MT17) was dissolved in 3 mL of a 10 mM HEPES buffer solution at pH 7, then the mixture was sonicated (30 s) in order to avoid particles agglomeration. Afterwards, 1 mL of a solution containing a 10 mM HEPES buffer and hhMb at pH 7 was added in order to reach a final protein concentration of 0.25 mg/mL. The experimental parameters for hhMb incorporation were chosen according to our previously reported results on the impact of buffer solution on protein adsorption[38].

The final mixed solution was shaken at room temperature for 96 h at 300 rpm on a 3500 Advanced Orbital Shaker. The adsorption was monitored at different time intervals by transferring 1 mL of solution in an Eppendorf tube and centrifuging it for 5 min at 4000 rpm. The amount of adsorbed proteins was calculated by analyzing the supernatant by UV-vis spectroscopy at the maximum of the Soret band of hhMb (λ_{max}= 408 nm) with a double beam Thermo Electron Evolution 500 UV-vis spectrophotometer. A 10 mM HEPES buffer solution was used as a reference. The experimentally determined molar extinction coefficient (ε= 129

1 $\mu M^{-1} cm^{-1}$) was used in the Lambert-Beer law to calculate the concentration from the

2 measured UV-vis absorption.

3 After the 96 h incorporation, the samples (hhMb-MT8 and hhMb-MT17) were filtrated and

4 washed three times with fresh buffer solution to remove possible non-adsorbed molecules.

5 After each washing step, the solution was analyzed by UV-vis to detect possible protein

6 leaching from the surface. In order to evaluate the hydration effect, the mesoporous TiO_2 with

7 adsorbed hhMb was dried for 15 min (hhMb-MT8_15 and hhMb-MT17_15) and 2 h (hhMb-

8 MT8_120 and hhMb-MT17_120) in an oven at 20 °C, immediately after washing. In this

9 manuscript, the naming of the samples is as follows: MT*x* is mesoporous titania with pore

10 diameter *x* nm, hhMb-MT*x*_*y* indicates incorporation of hhMb in MT*x* titania and drying for *y*

11 minutes in an oven at 20 °C.

12 **Catalytic Assay**

13 The catalytic activity of hhMb is usually evaluated through the peroxidase activity, attributed

14 to the heme group, toward ABTS in the presence of H_2O_2.

15 The assay solution was prepared dissolving 10 mg of hhMb-MT8 and hhMb-MT17 (with

16 different drying time) in 2 mL HEPES solution at pH 7. All samples with incorporated hhMb

17 were used immediately after the drying step in the oven. Afterwards, 1.5 mL of 1 mM H_2O_2

18 and 0.5 mL of 0.5 mM ABTS were added. Then, the final solution was shaken at 300 rpm at

19 room temperature for 24h. The interconversion of ABTS (λ_{max}= 340 nm) into its radical cation

20 ABTS$^{\bullet+}$ (λ_{max}= 414 nm)[39] was monitored in different time intervals by UV-vis spectroscopy

21 analysis of the supernatant after centrifugation, as explained above. To validate the ABTS

22 assay, blank tests were performed dissolving 10 mg of the titania materials without adsorbed

23 proteins (MT8 and MT17) in 2 mL HEPES and then adding H_2O_2 and ABTS as described.

24 **Characterization**

1	The N_2 sorption analysis was performed using a Quantachrome Quadrasorb SI automated gas

2	adsorption system with an AS-6 degasser. Before starting the measurement, TiO_2 samples

3	with (hhMb-MT) and without (HEPES-MT) adsorbed hhMb were outgassed at 25 °C for 16 h.

4	Then, the analysis was performed at -196 °C. The Brunauer-Elmet-Teller (BET) multipoint

5	method was used to calculate the specific surface area (S_{BET}). The total pore volume (Total V_P)

6	was calculated from the adsorption at P/P_0 0.95.

7	The DRIFT spectra were acquired using a Nicolet 6700 FT-IR spectrometer. The samples were

8	mixed (2 wt %) with dry KBr and pure KBr was used as reference. For each sample, 200 scans

9	were averaged and a resolution of 4 cm^{-1} was applied. The error on the amide band I/II ratio

10	was calculated by collecting the DRIFT spectrum of three different samples. The second

11	derivative of the spectra was calculated using the Savitsky-Golay algorithm for a 13 data point

12	window using the spectra analysis software OMNIC[40]. In addition, the *in-situ* DRIFT spectra of

13	the support materials were collected using a DTGS detector after degassing in vacuum and

14	heating at 150 °C *in-situ* for 30 min. Moreover, water sorption measurements were performed

15	using a Quantachrome iQ automated gas sorption system with the manifold heated to 50 °C.

16	The samples were degassed under high vacuum conditions at 150 °C for 16 h, before

17	measuring the water isotherms at 22 °C. The UV-vis DR analysis was performed on a Thermo

18	Electron Evolution 500 UV-vis spectrophotometer equipped with an integrating sphere. The

19	samples were diluted to 2% weight with dried KBr and pure KBr was used as a reference. The

20	spectra were acquired in the range 350-700 nm with a scan speed of 120 nm/min. Zeta

21	potential measurements were performed using a Zetasizer Nano ZS from Malvern Panalytical

22	with a He-Ne laser (633 nm). The samples (1 g/L) were analyzed in a folded capillary cell

23	(polycarbonate) with gold coated electrodes. An aqueous sodium chloride solution (10 mM)

24	was used as medium. The temperature was kept constant at 25 °C.

1 X-band continuous wave (CW) EPR measurements were performed on a Bruker ESP300E

2 spectrometer with a microwave (mw) frequency of ~9.44 GHz. The spectrometer is equipped

3 with a liquid Helium cryostat (Oxford Inc.), allowing to operate from room temperature down

4 to 2.5 K. The EPR spectra were recorded at 10 K with a modulation frequency of 100 kHz, a

5 modulation amplitude of 0.5 mT and a microwave power of 0.5 mW. To avoid paramagnetic

6 oxygen as a background signal, a vacuum pump was attached to the EPR tube during the

7 measurements. The EPR spectra are simulated using the MATLAB toolbox Easyspin[41].

8 A high resolution (precision of 0.05% wt) vertical thermobalance Q5000IR (TA instrument)

9 coupled to a Thermostar^{TM} GSD 301T quadrupole mass spectrometer (Pfeiffer Vacuum) was

10 used for TGA-MS analysis of hhMb-MT8_15 (12.7860 mg), hhMb-MT8_120 (15.0160 mg),

11 hhMb-MT17_15 (6.9970 mg) and hhMb-MT17_120 (8.1510 mg). The HRTGA-MS coupling is

12 featured with a temperature-controlled gas line (quartz capillary, length= 1.2 m, 250 ^{o}C).

13 The outlet port of thermobalance and the inlet port of the mass spectrometer are separately

14 heated to avoid cold spots. TGA-MS analysis was performed in a He atmosphere (60 mL/min)

15 at a heating rate of 20 ^{o}C/min from 25 ^{o}C to 625 ^{o}C. Mass spectra were continuously collected

16 (3 mass spectra/min) in EI mode, full scan mode, within a mass range of 10-200 amu.

17 **Results and Discussion**

18 **Surface Characterization of MT8 and MT17**

19 The protein-surface interactions have a large impact on the conformation of the adsorbed

20 molecules and they are strongly dependent on the properties of the solid surface, e.g.

21 hydration, charge and morphology[42–44]. Therefore, in order to avoid misguided interpretation

22 of the experimental results due to differences in the surface chemistry of the two titania

23 materials, we first report on several surface features of MT8 and MT17 prior to describing

1   their differences in hhMb adsorption, stability and activity. Here we focus on the surface

2   charge, hydrophilicity and chemistry. We refer to our previously published work for details

3   about the structural characteristics[35].

4   The in-situ DRIFT spectra (vacuum at 150 °C for 30 min) of MT8 and MT17 (Figure 1) show at

5   high wavenumber a broad band extending from ca 3600 cm^{-1} to approximately 2600 cm^{-1}

6   attributed to the surface hydroxyl groups and vibrations of un-dissociated water, and a well-

7   defined peak at 3660 cm^{-1} attributed to the isolated or weakly interacting surface hydroxyl

8   groups[45].
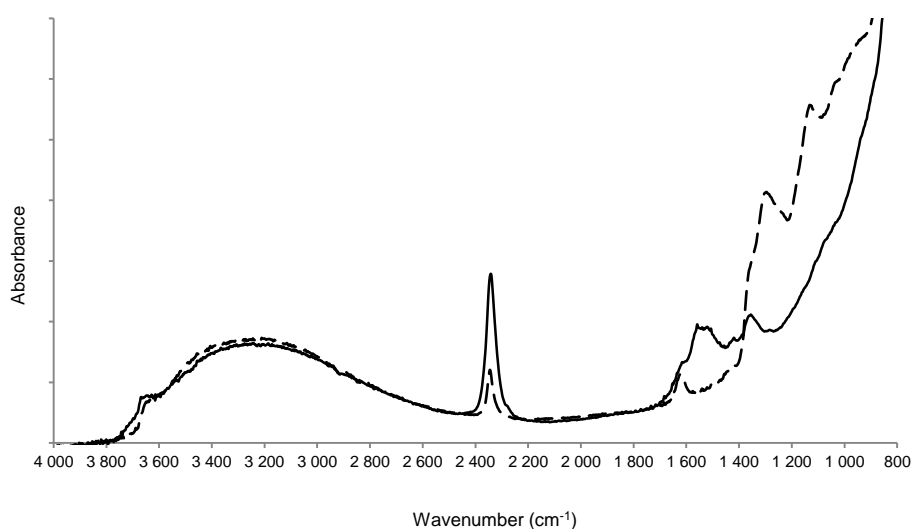
9

10   *Fig. 1. In-situ DRIFT spectra of MT8 (solid line) and MT17 (dashed line). The samples were degassed and heated at 15 0ºC for*
11   *30 minutes before measuring.*

12   It is important to note that even though no substantial differences are observed in this region

13   between the two samples, clear differences are present below 1700 cm^{-1}. The *in-situ* DRIFT

14   spectra show a complex pattern of bands originating from interaction with water and the

15   presence of carbonate-like species on the surface of MT8 (the latter having peaks at 1578 and

16   1513 cm^{-1})[46]. Moreover, sulfate anions can be observed on the surface of MT17 (peaks at

17   1302, 1130 and 1040 cm^{-1}) as already discussed in our previous work on the synthesis of

18   mesoporous TiO$_2$[35]. Surface contaminants are difficult to avoid when preparing materials with

different pore properties (e.g. different pore size) as additives need to be applied, but their

presence on the surface have been reported to influence hydration and dehydration of

specific surface species[47]. Nevertheless, the water sorption isotherms (Figure S1, Supporting

Information) show similar monolayer capacity for MT17 and MT8 at low P/P_0. This is important

as the hydrophilicity of the substrate surface is a crucial factor in determining the activity of

the adsorbed proteins[48]. In addition, the zeta potential measurements (Figure S2, Supporting

Information), although showing different points of zero charge, indicate similar surface charge

for MT17 and MT8 at pH 7 (the applied pH of protein incorporation).

Overall, the results suggest that, although local differences in interaction and hydration

cannot be excluded due to the presence of carbonate and sulfate species on MT8 and MT17,

respectively, the two samples exhibit similar water sorption behavior and surface charge (at

the applied pH).

Therefore, although an impact caused by local dissimilarities in surface chemistry cannot be

excluded, differences in the hhMb adsorption and stability are expected to be due mainly to

the different confinement (pore size) and (de)hydration experienced by the proteins.

Adsorption of hhMb onto the Mesoporous Titania: Formation of hhMb-MT8 and hhMb-MT17

Figure 2 shows the adsorption isotherms representing the adsorption of hhMb on MT8 and

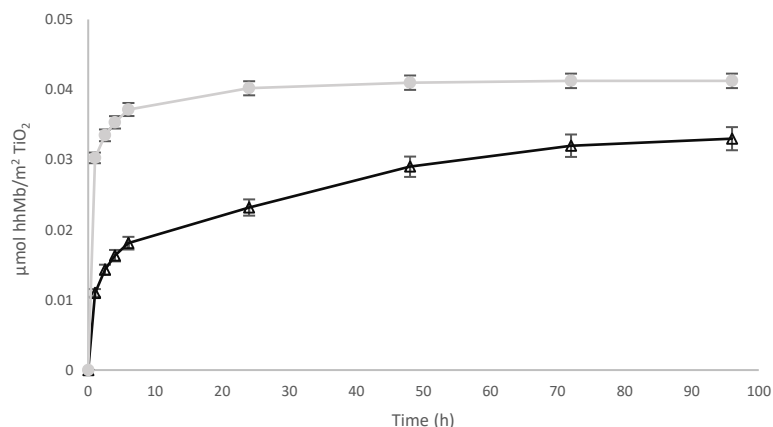MT17 (μmol of hhMb per m^2 of mesoporous TiO_2) as a function of time.

Fig. 2. Adsorption isotherm of incorporating hhMb on MT17 (●) and MT8 (Δ) in HEPES buffer 10mM pH 7. The error bars were calculated on

a set of three measurements.

4   MT17 shows the most efficient protein adsorption (about 90% of proteins are incorporated

5   within 6 h). The MT8 sample shows a less efficient uptake, although still 80% of the hhMb

6   proteins are adsorbed over 72 h. The enhanced loading capacity for samples with larger pores

7   has been previously reported to originate from a more efficient protein diffusion into the

8   pores[49,50]. No protein desorption was observed during the washing steps performed at the

9   end of the isotherms.

10   The successful incorporation of hhMb into the mesoporous TiO_2 is confirmed by the N_2

11   sorption data (Table 1 and Fig. S3, Supporting Information). The pore volume (V_P) reduction

12   upon adsorption can be compared to the volume of the incorporated hhMb (assuming a molar

13   volume of hhMb of ca 1.3×10^4 cc/mol)[51]. Nevertheless, it has to be noted that some volume is

14   also taken by differences in the remaining water and HEPES that is left in the samples (HEPES-

15   MT17 and HEPES-MT8), as degassing was only performed at 25 °C. The difference in volume

16   reduction (HEPES compared to hhMb), in addition to the small decrease of the BET surface

17   area (S_{BET}), suggests that hhMb diffuses and adsorbs inside the pore network[52]. This is

18   confirmed by the t-plot analysis of the N_2 sorption isotherms of the two materials before

1 (HEPES-MT17 and HEPES-MT8) and after (hhMb-MT17 and hhMb-MT8) hhMb adsorption. In

2 fact, the t-plot shows that the loss of external surface area (S_{ex}) of the material represents only

3 30% of the loss of the total surface area upon protein adsorption.

4 *Tab. 1. Results of the N_2 sorption analysis of MT8 and MT17 after being dissolved in free (no hhMb) buffer solution (HEPES-MT) and upon*

5 *adsorption of hhMb (hhMb-MT17 and hhMb-MT8). All samples were degassed at 25 °C for 16 h.*

Sample	S_{BET} (m²/g)	S_{ex} (m²/g)*	S_{meso} (m²/g)*	Total V_P (cc/g)
MT17	140	36	104	0.60
HEPES-MT17	125	30	95	0.58
hhMb-MT17	108	25	83	0.48
MT8	133	27	106	0.31
HEPES-MT8	121	22	99	0.30
hhMb-MT8	108	18	90	0.22

11 * Calculated using the t-plot analysis

12 When varying the amount of the mesoporous TiO_2 relative to the concentration of hhMb, a

13 Langmuir isotherm-like curve is observed for both hhMb-MT8 and hhMb-MT17 (Figure S4,

14 Supporting Information) suggesting mainly a monolayer coverage. However, as shown by

15 Latour, most of the protein adsorption processes do not fulfill the prerequisites for a Langmuir

16 adsorption process[53], as changes in the conformation and reorientation, as well as the

17 interaction between the adsorbed proteins, significantly deviate from the dynamic

18 equilibrium adsorption process.

19 **Effect of (de)hydration and Confinement on the hhMb Structure.**

20 FT-IR spectroscopy is a valuable tool for the investigation of the secondary structure of the

21 protein[54], and it has been previously used to detect conformational changes of proteins upon

22 adsorption in mesoporous TiO_2[55,56]. The amide band I and II of the DRIFT spectra of the

23 different samples are shown in Figure 3. The amide band I (mainly due to the C=O stretching

24 mode) and the amide band II (combination of NH in-plane bending and CN stretching) of hhMb

1   are located at 1660 cm^{-1} and 1542 cm^{-1}, respectively[57]. The intensity ratio between the

2   maxima of the amide band I and II in lyophilized hhMb powder is 1.1±0.1 in according to what

3   is reported for hhMb in solution[44]. The enhanced intensity ratio (1.3±0.2) of the two bands for

4   hhMb-MT8_15 and hhMb-MT17_15 is an indication of differences in the structure of the

5   adsorbed proteins when compared with the lyophilized hhMb[58]. In addition, the ratio of the

6   amide I/II band increases further for hhMb-MT8_120 (1.5±0.2) and hhMb-MT17_120

7   (1.6±0.2), suggesting more extended structural rearrangements of the protein backbone when

8   the drying time increases. However, a simultaneous influence of the spectral contribution of

9   adsorbed water (peak at 1630 cm^{-1}) on the ratio between the amide band I and II in the

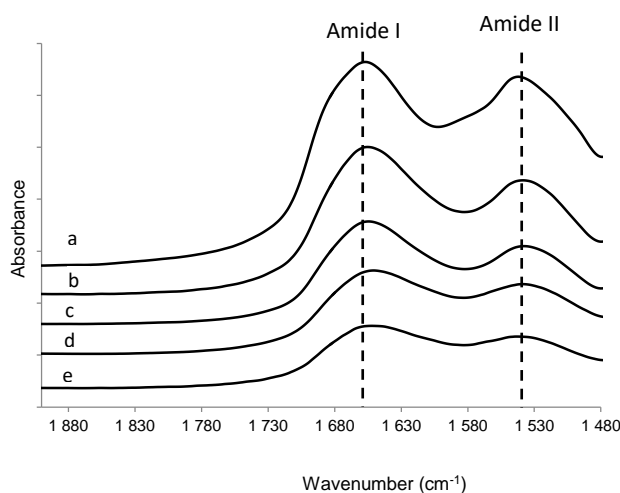10   different samples cannot be excluded.

11

12   *Fig. 3. Magnification of the DRIFT spectra in the region of the amide bands I and II (offset 0.05) of lyophilized hhMb powder (a), hhMb-*

13   *MT17_15 (b), hhMb-MT17_120 (c), hhMb-MT8_15 (d) and hhMb-MT8_120 (e) after washing and drying at 20 °C.*

14   The IR region of the amide band I is sensitive to conformational changes due to the C=O

15   stretching mode, which is dependent on the strength of the hydrogen bonds between the

16   carboxyl and the amino groups of the peptide structure. Therefore, this band is composed of

17   a superposition of signals originating from the different contributions of α-helices, β-sheets

18   and random coils. Hence, analysis of the amide band has been described as a valid tool to

1 monitor the folding/unfolding of a protein[58–60]. This can be done by curve fitting (i.e.

2 deconvolution of the spectrum), but it relies on arbitrary deconvolution parameters and the

3 procedure often leads to incorrect spectral interpretation[40]. Therefore, a more qualitative

4 approach in which the second derivative of the IR spectrum is considered is often preferred.

5 This derivative spectrum allows to easily assess changes in the amide band I that are less clear

6 in the IR spectrum. However, it has to be noted, as already discussed, that this region of the

7 DRIFT spectra is influenced by the contribution of the adsorbed water, and thus only

8 qualitative analysis of the secondary structure can be performed.

9 We calculated the second derivative of the amide I band of the different samples (Figure 4) to

10 further investigate possible structural changes of hhMb caused by the differences in
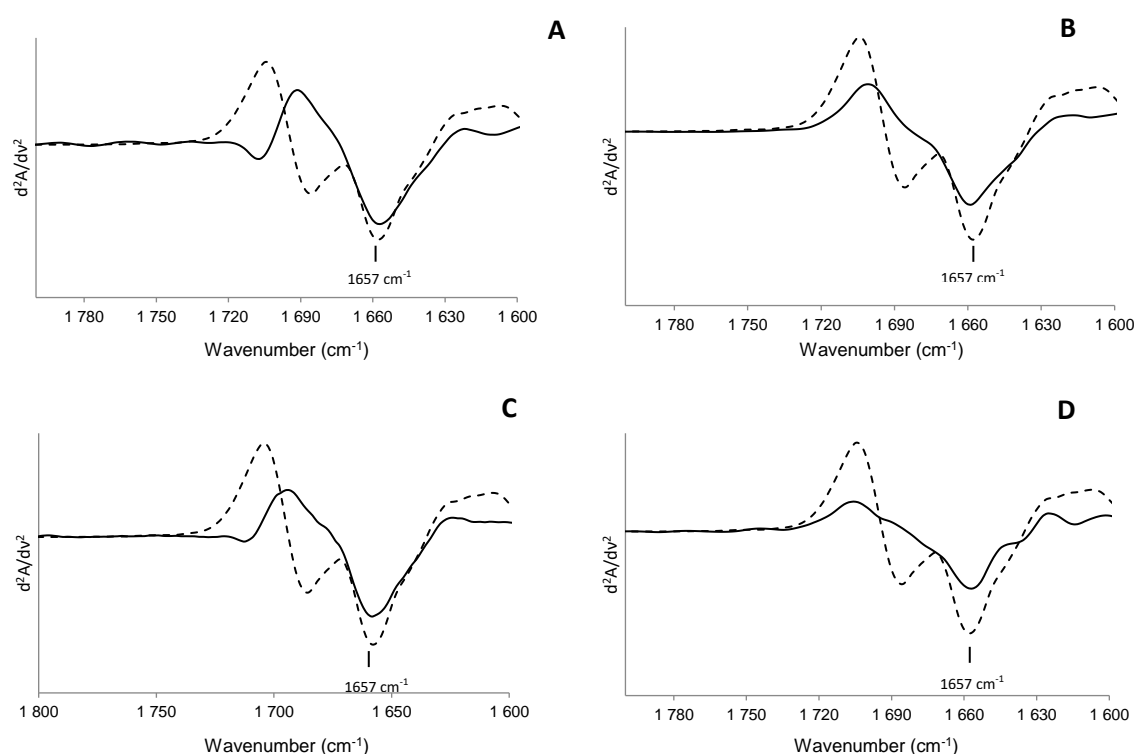
11 confinement and (de)hydration.

14 *Fig. 4. Second derivative DRIFT spectra of the amide band I of lyophilized hhMb powder (dotted line) and of hhMb-MT8_15 (A, solid line),*

15 *hhMb-MT8_120 (B, solid line), hhMb-MT17_15 (C, solid line) and hhMb-MT17_120 (D, solid line) after washing and drying at 20 °C.*

The second derivative of the amide band I of lyophilized hhMb reveals the two secondary structural features of this protein: α-helices (band at 1657 cm^{-1}) and peaks in the region 1670-1720 cm^{-1} attributed to the random-coils[61]. As the structure of hhMb is composed of 70-80% α-helix and 20-30% of random coil, with no β-sheet structure[62], the α-helical band at 1657 cm^{-1} is of particular interest. This minimum appears in the same position for all the four samples with incorporated proteins, although distorted in hhMb-MT8_120 (where a small shift is also detected) and hhMb-MT17_120. This suggests an important influence of the (de)hydration on the structure of the adsorbed hhMb since the α-helical structure seems to be better preserved for shorter drying times.

However, all samples present remarkable spectral changes compared to the lyophilized protein in the range assigned to the random-coil structure. In particular, the second derivative analysis of the amide band I evidences structural changes as a consequence of the adsorption into the mesoporous TiO$_2$. In addition, the changes in the region 1690-1696 cm^{-1} and 1620-1640 cm^{-1} (although this region has to be carefully evaluated as it might be influenced by the contribution of the adsorbed water) suggest the formation of β-sheets similarly to what is observed for hhMb adsorbed on silica[60]. This is expected as the majority of the proteins undergoes conformational changes to some extent when adsorbing on a solid surface[63,64] to minimize the interaction energy with the solid surface. In particular, in case of globular proteins as hhMb, the loss of α-helix motives has been reported for albumin upon adsorption on a gold surface[43] and hemoglobin interacting with silica[65]. In the latter, the interaction between amino acids on the α-helices and the hydroxyl surface groups is proposed to be responsible for the transition between α-helix and β-sheet.

Therefore, the second derivative DRIFT analysis hints to changes in the secondary structure, particularly in the random-coil portion, of hhMb mainly due to the confinement of the protein inside the pores of mesoporous TiO_2. The type of structural rearrangements depends, however, on both the pore size and (de)hydration. In addition, important differences are observed between samples dried for different times with hhMb-MT8_15 and hhMb-MT17_15 presenting better preserved α-helix structures. This suggests an important effect of the water content inside the pores on the hhMb secondary structure, which is in line with earlier observations on the effect of surface hydration on the structure of apomyoglobin in nanoporous organosilica sol-gel glasses[66]. However, it is reasonable to assume that no structural water holding together the hhMb structure is removed during the drying time as this would have a strong impact on the DRIFT spectra. In particular, dehydration of the protein would lead to a serious loss of α-helix motives (up to 90%) and a shift of the α-helix band in the second derivative spectra towards higher wavenumbers[67,68].

Nevertheless, differences in the structure of hhMb upon adsorption in MT8 and MT17 due to local differences in the surface chemistry of the two titania materials (see Fig. 1) cannot be excluded.

As the protein stability can also be determined by studying its disruption[69], we performed TGA-MS to further investigate the effect of hydration and confinement on the hhMb structure. The results indicate that the thermal degradation of hhMb adsorbed into mesoporous TiO_2 is influenced by both the pore size and the drying time.
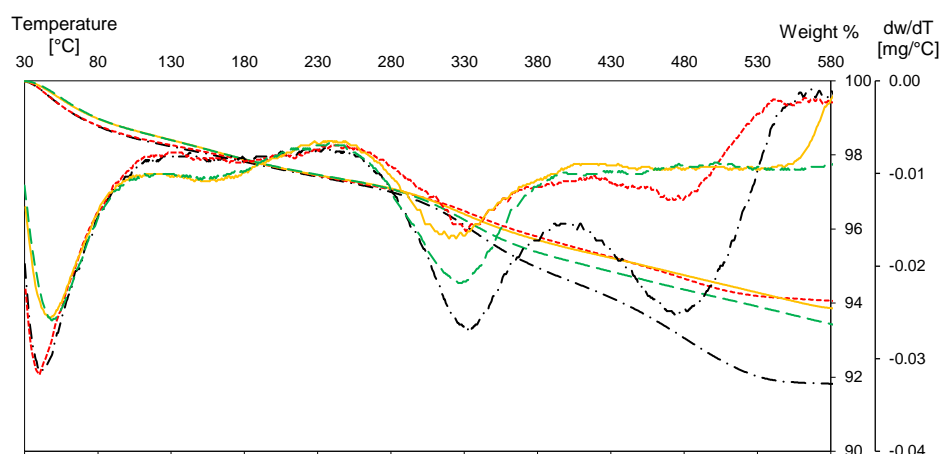
4 Four different weight losses are observed in the DTG-TGA profiles of all samples (Figure 5).

5 The mass spectroscopic analysis (Fig. S5-8, Supporting Information) attributes the two weight

6 losses below 200 °C to the adsorbed water (characteristic mass-to-charge ratio (m/e) 17 and

7 18 in TGA-MS). The shift and low intensity observed in the second DTG peak maximum (158

8 °C and 170 °C for hhMb-MT8 and hhMb-MT17, respectively) is likely due to the difference in

9 water interaction with the surface[47], as confirmed by the DTG profiles of the samples without

10 adsorbed hhMb (Fig. S9, Supporting Information)

11 The two weight losses above 250 °C are attributed to the pyrolysis of hhMb[70]. All samples

12 show a prominent DTG peak at about 330 °C. It is important to note, that for the material with

13 the largest pores (hhMb-MT17_15/120), this peak is slightly shifted toward higher

14 temperature (334 °C) when compared to 328 °C to hhMb-MT8-15/120.

15 Even though 20% less proteins were absorbed in the 8 nm pore size material (hhMb-MT8), the

16 weight loss shown by the TGA profiles in the range 200-400 °C is similar for hhMb-MT8_15

17 and hhMb-MT17_15 (2.0%). On the other hand, higher weight loss values are observed in the

18 TGA curves of hhMb-MT8_120 (2.3%) and hhMb-MT17_120 (3.0%) despite the fact that the

only difference is a longer drying time and thus the same amount of proteins are present in the material as in case of the short drying time. This suggests that depending on the drying time, different degradation pathways occur induced by the differences in (de)hydration of the adsorbed hhMb. The main products observed in the mass kinematograms of all samples in this temperature range are H_2O (m/e 17 and 18), CO_2 (m/e 44) and CH_2O (m/e 30). Water at enhanced temperature has to be considered as a result of thermal degradation, e.g. elimination reactions.

In addition, clear differences in the relative amount of different side products are observed in the region between 200 and 400°C, depending on both the pore size and the drying time. In particular, the most abundant side products detected in the kinematograms of hhMb-MT8_15 and hhMb-MT8_120 are small hydrocarbons with m/e 27, 39 and 41 (probably C2 and C3 fragments) and C_2H_5O (m/e 45). The amount of those fragments is different between hhMb-MT8_15 and hhMb-MT8_120, suggesting an influence of the drying time on the hhMb degradation. The same side products are observed for hhMb-MT17_120 (Figure S8, Supporting Information), although in lower concentration. On the contrary, fragment ions with m/e 41 and 45 are only detected in the kinematogram of hhMb-MT17_15 (Figure S7, Supporting Information).

A second weight loss is observed for all samples in the range 400-600 °C. Again, the TGA curve shows similar weight losses for hhMb-MT8_15 and hhMb-MT17_15 (1.5%), while more prominent weight losses are observed for hhMb-MT8_120 (2.3%) and hhMb-MT17_120 (2.8%).

The mass spectroscopic analysis reveals that the main residues for all samples are CO_2 and CH_2O. In addition, other side products (m/e 27 up to m/e 64) similar to those discussed

previously are still detected. It is important to note that fragment ions with higher mass (m/e

> 70) are observed for all samples. Those ions probably arise from partial fragmentation of the

peptide chain and strongly contribute to the weight losses shown in the TGA profiles.

Of particular interest are the two ions with m/e 48 and 64 detected in the kinematograms

assigned to SO and CH_3SOH arising from the fragmentation of the two methionine of hhMb[71].

They are visible in different temperature ranges for the different materials. In case of hhMb-

MT8_120 they only appear below 400 °C (328 °C), while in case of hhMb-MT17_15 and hhMb-

MT17_120 they are solely observed above 400 °C. Moreover, in hhMb-MT8_15 these signals

are absent.

The differences observed in the TGA-MS are a valuable proof of the influence of both

(de)hydration and confinement on the structural rearrangement of hhMb[72]. In particular, the

smaller weight losses observed for hhMb-MT8_15 and hhMb-MT17_15 above 250 °C suggest

a different degradation and, thus, a different folding and/or interaction with titania of the

hhMb after drying for shorter time. Similarly, the different products detected for these two

samples indicate different mechanisms of thermal degradation of hhMb upon incorporation

in pores with different sizes. This agrees with NMR findings that water (hydration and internal

water molecules) and hydrogen bonds play an essential role in the different routes through

which protein (un)folding occurs[73]. Furthermore, Monte Carlo simulations show that

confinement reduces the entropy of the unfolded state by limiting the conformational space

available to the unfolded ensemble[74], explaining the different unfolding pathways and hence

thermal degradation pathways that will occur in MT8 and MT17.

The interplay of confinement and (de)hydration effects in the stability of hhMb is also

confirmed by the second derivative DRIFT analysis, showing that the partial loss of ordered α-

helical content of hhMb upon longer drying times occurs to a different extent and via formation of other types of structures in hhMb-MT8_120 and hhMb-MT17_120 (see Figure 4).

As stated above, the protein unfolding upon incorporation in a porous substrate depends also on the interactions between the protein and the pore wall. In its native state, hhMb has a hydrophilic surface with the hydrophobic segments buried inside the globular structure. As a consequence of the adsorption inside the pores the external hydrophilic residues might interact with the OH groups of the TiO_2 surface, leading to a partial rearrangement of the external amino-acid residues of hhMb accountable for the differences observed in the DRIFT spectra of lyophilized hhMb powder and of hhMb incorporated samples.

Clearly, such rearrangement is expected to be strongly prevented by the space constriction upon adsorption in MT8. However, hhMb has a maximum diameter of 5 nm, smaller than the pore diameter of MT8. Therefore, the differences in hydration of hhMb-MT8_15 and hhMb-MT8_120 can play a key role in local changes and resulting differences in thermal behavior. In large pore materials, such as MT17, more extensive rearrangements of the protein can take place upon drying as more "space" is present in the porous structure. Hence, small changes in the D- and/or H-helix orientations, on which the two methionine residues are situated, might be at the basis of the altered thermal degradation in the MT17 irrespective of the (de)hydration. One possible scenario is the small D-helix, positioned next to the flexible CD-loop at the surface of the protein, being one of the domains that is easily influenced by contact with the titania surface. Furthermore, although both (de)hydration and confinement clearly play a role, their impact seems to be different. Once again, we stress that impact of the different surface chemistry between MT8 and MT17 materials cannot be ruled out and it

1   might enhance the difference in the structure of the adsorbed hhMb in the two titania

2   materials.

3   To further investigate the effect of confinement and (de)hydration on the hhMb structure, we

4   performed UV-vis DR (Figure S10, Supporting Information). Although a blue shift of the Soret

5   peak may point to changes in the physical environment of the heme, resulting from unfolding

6   of the hhMb structure[75,76], the UV-vis DR data have to be interpreted with care, since there is

7   overlap with the tail of the absorption peak of the MT8 and MT17 materials, which could lead

8   to an apparent shift.

9   A much better insight in the heme pocket region can be obtained from EPR. This technique

10   provides a sensitive measure to changes in the heme group and heme coordination. The aquo-

11   met form of hhMb consists of a high-spin (HS) ferric heme iron atom which is six-coordinated

12   by the proximal F8His and a distal water molecule. The aquo-met form of hhMb can be

13   described by an effective S = 1/2 system with g-values $g_{x,y}^{eff}$ = 5.92 and g_z^{eff} = 1.997.[77] Removal

14   of the heme-bound water molecule or a change in the heme environment leads to shifts,

15   splitting or broadening of the HS component in the low-field part of the EPR spectrum.

16   Replacement of the distal water by a strong base, such as hydroxide or an imidazole, gives rise

17   to a low-spin (LS) ferric state with a different EPR signature.

18   Figure 7 represents the EPR spectra of the powders hhMb-MT8_15/120 and hhMb-

19   MT17_15/120. All spectra show the main characteristic features of the HS (S = 5/2) ferric heme

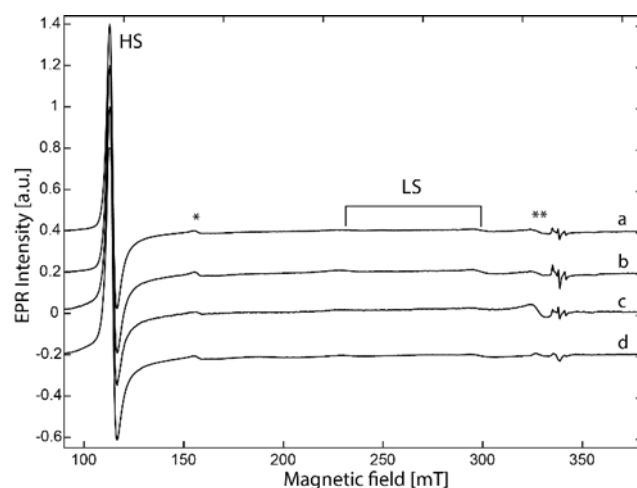20   in the aquo-met form and those of a LS form.

21

The spectra shown in Figure 6 are very similar, indicating that the incorporated protein molecules exhibit no major differences in protein structure near the heme center for the different hybrid materials. Nevertheless, hhMb-MT17_15/120 shows a slightly broader signal in the low-field part of the HS contribution than hhMb-MT8_15/120 (Figure S11, Supporting Information). The latter in turn exhibits somewhat more broadening EPR spectrum as found for a frozen solution of hhMb (Figure S11, Supporting Information). The broadening of the EPR signal points to a larger variation of the zero-field splitting parameters that stems from an increased local variability in the heme environment and thus subtle local changes in the protein structure. The line width follows the confinement trend: more peak broadening for the titania with larger pore size (larger conformational space). Furthermore, drying for 2 h does not cause loss of the axially bound water molecule on the heme iron, since this would lead to much more severe line deformation and splitting of the lines. The mild drying conditions probably prevent the loss of the bound axial water ligand. Even though the DRIFT spectra indicate structural changes for both drying times (Figure 4), EPR shows that these changes do not affect the heme-pocket. The decrease and alteration of the random coil structure appear to be occurring far enough from the heme to not influence the heme-pocket

23

region of the HS form. The loop areas in hhMb are shown in Figure S12, Supporting Information.

Furthermore, a clear EPR signal due to a low-spin (LS) ferric heme center is detected at g_z ~ 2.97 and g_Y ~ 2.254 in all samples (Figure 6, Figure S13, 14, Supporting Information, shows the spectrum of the LS form in detail together with its simulation). We have shown earlier that this indicates that in a fraction of the proteins, the heme-bound water molecule is replaced by ligation of the distal His-64 located on helix E to the heme iron atom[38]. The formation of this bis-histidine ligated form is promoted by the interaction of the protein with the titania material[38]. Via spectral simulations the relative contribution of the HS and LS heme forms to the EPR spectra can be determined (Figure S13, 14, Supporting Information). The contribution of the LS heme iron form comprises about 39% of the spectrum for all powders in spite of the apparent weak intensities of these LS signals. The LS form is not found in the EPR spectra of the frozen solution and is related to confinement effects as showed earlier[38]. The shift of the E-helix may be related to particular altered structures observed in the FT-IR spectra.

In the high-field part of the EPR spectra of Figure 6, extra signals are observed, that are also found in pure titania MT8 (Figure S15, Supporting Information). This part mainly contains contributions of oxygen-containing radical, like O_2^- ($g > 2$) and of Ti^{3+} ($g < 2$) in the mesoporous titania, generated from the calcination at high temperature (>300 ^{o}C)[78].

Peroxidase Activity of Incorporated hhMb

As the preservation of the protein activity upon adsorption is a key issue in protein incorporation, it is of fundamental importance to investigate the possible effect of confinement and (de)hydration on the activity of the adsorbed hhMb.

1 The one-electron oxidation of ABTS into the radical-cation ABTS$^{\bullet+}$ by hhMb in presence of

2 hydrogen peroxide has already been used to test the catalytic activity of incorporated

3 proteins[11,12]. The reaction occurs via the heme in three different steps[39], starting with

4 oxidation of iron (III) to an oxoiron(IV)-porphyrin π-cation by hydrogen peroxide and the

5 subsequent two-step reduction to oxoiron(IV) (1st step) and Fe(III) (2nd step), forming two

6 molecules of ABTS$^{\bullet+}$. The blank tests performed with titania materials without adsorbed hhMb

7 (MT8 and MT17) show no ABTS conversion in absence of the proteins. The values for the

8 turnover number k_{cat} (μmol ABTS$^{\bullet+}$ produced per second per μmol of hhMb) show differences

9 in activity for hhMb depending on both the pore size and the drying time (Figure 8).
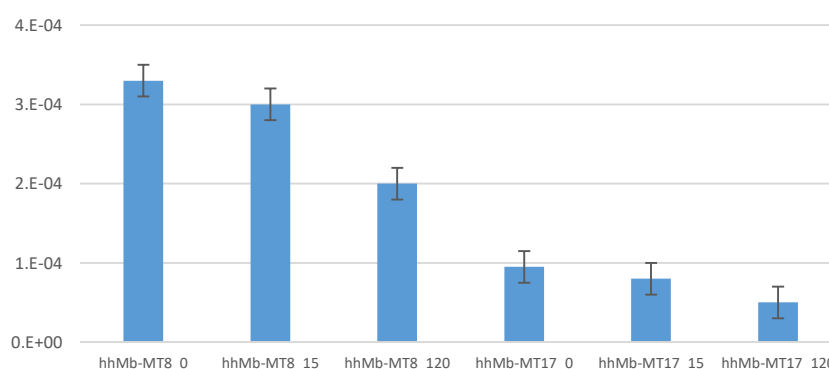
10

11 *Fig. 8. Plot of k_{cat} as a function of the pore size and the drying time. The error bars were calculated on a set of three measurements.*

12 As the catalytic constant was calculated per mass of hhMb, the different values cannot be

13 related to differences in the amount of adsorbed hhMb. It has to be noted that the hhMb

14 activity in all samples is strongly reduced when compared with the activity of the proteins free

15 in solution ($k_{cat} \approx 10^{-2}$ s^{-1}, data not shown). The decrease of the catalytic activity is a common

16 phenomenon for incorporated proteins due to inaccessibility of part of the proteins inside the

17 pores[79] or partially deactivation upon adsorption on the solid surface[80]. Furthermore, a limited

18 diffusion of the substrate towards the protein and/or diminished accessibility of the heme

19 pocket, not due to structural alterations of the heme itself, could also be responsible for the

observed decrease in activity. In case of MT8 and MT17, the different surface chemistry (see Fig. 1) might also play a role although the surfaces of the two samples present comparable water sorption capacity.

Therefore, the substantially different values of k_{cat} observed must be connected to the different hydration and confinement experienced by the proteins. In fact, the differences between hhMb-MT8_15 (3×10^{-4} s^{-1}) and hhMb-MT17_15 (8×10^{-5} s^{-1}) and between hhMb-MT8_120 (2×10^{-4} s^{-1}) and hhMb-MT17_120 (5×10^{-5} s^{-1}) are expected to be due to the different confinement. This is in agreement with previous results showing enhanced activity for proteins encapsulated in small pores[14,81,82]. In fact, the better catalytic activity observed for hhMb adsorbed in smaller pores (hhMb-MT8_15 and hhMb-MT8_120) might be due to the better accessibility of the hhMb, which is not able to diffuse in the inner part of the pore network[81,82], allowing easier diffusion of the substrate to the heme. This is in agreement with the lower protein loading in MT8 materials (Figure 1).

On the other hand, the somewhat smaller differences between the catalytic activity of hhMb-MT8_15 and hhMb-MT8_120 and between hhMb-MT17_15 and hhMb-MT17_120 are likely due to the structural differences induced by the changes in hydration.It shows that drying-induced structural changes are not reversible. Indeed, for the catalytic assay, the samples are dissolved in HEPES buffer. If the dehydration effect would be reversible upon rehydration, the same activity would be found for the materials with 15 min or 2 h drying. This is supported by the higher catalytic activity observed for non-dried samples (hhMb-MT8_0 and hhMb-MT17_0). It has to be noted that, with the exception of EPR, the techniques we used to characterize the hhMb structure upon adsorption and drying require dry samples. Therefore the non-dried samples are only used here to further evidence the importance of the hydration.

1 The here observed importance of hydration is in agreement with the reported improved

2 protein activity and enhanced resistance to extreme pH values when proteins are entrapped

3 in strongly hydrated material[83]. Possibly, the drying-induced structural changes in hhMb affect

4 the diffusion pathways and overall accessibility of the heme center, since EPR results indicate

5 that the active heme center seems to be less affected (see EPR analysis).

6 **Conclusion**

7 Changes in conformation are expected when a protein adsorbs into a porous network due to

8 the materials properties (i.e. surface chemistry and pore size), differences in (de)hydration

9 and protein properties. Here we focused on the impact of (de)hydration and pore size *via*

10 investigation with a complementary set of techniques. Although the two titania materials used

11 in this work present differences in surface chemistry, inducing local differences in the water

12 content and interaction, the two surfaces present similar water sorption capacity and charge

13 (at the applied pH), making them suitable substrates to study the impact of hydration and

14 confinement on the protein structure

15 The different techniques evidence that both (de)hydration and confinement induce changes

16 in the proteins, although their impact is different. The use of EPR and DRIFT allows to exclude

17 that the water molecules from the heme cavity or structural water holding together the hhMb

18 secondary structure are removed during the drying time. Therefore, it is reasonable to assume

19 that the water molecules removed during the drying time are desorbing from both the titania

20 surface and the hydration shell of hhMb. However, it is difficult to quantify the contribution

21 of each.

22 In fact, an exact calculation of the water content is not straightforward if not misleading. First,

23 although the water amount can be calculated for the materials without adsorbed proteins,

there is no evidence of the origin of the water molecules loss observed in the TGA (hydration shell of hhMb or titania surface). Second, the adsorption of hhMb might lead to a different water content in the titania materials as a consequence of the presence of the protein inside the pores and its interaction with the pore walls. In addition, the local differences in the water content on the two titania materials might lead to a different water evaporation from the surface. This could however not be characterized with the current techniques.

On the other hand it has to be considered that also water from the hydration shell is likely to be removed during the drying step. This is strengthened by the differences in the external loops conformation of the hhMb structure (DRIFT). In fact, if the hydration shell of hhMb becomes thinner (as a consequence of drying), it is possible for the hydrophilic external loops to have stronger or more extended interactions with the titania surface hydroxyl groups, causing the conformation differences, although more detailed studies are required to confirm this and identify their exact nature.

However, as clearly shown by TGA-MS and the ABTS assay, the drying time has a strong impact on the protein degradation and on the protein activity, suggesting evaporation of water from the interface between protein and titania (protein hydration shell and/or titania surface) and an influence of such water loss on the hhMb outer structure and/or conformation.

Since the heme region is essential for the catalytic function and only experienced very minor impact, the observed differences in peroxidase activity will be primarily due to a change in the accessibility of the proteins to the substrate, caused by the peripheral structural changes and pore confinement. Earlier studies suggested that smaller pore sizes lead to less deep penetration of the proteins in the pore network of the material and, hence, a better accessibility of the proteins to substrates. This is confirmed in our study, as the smaller pore

size, loaded with proteins, shows higher activity. Furthermore, it is clear that more extensive

drying reduces the activity of the protein irreversibly, probably due to the higher substrate

hindrance due to partial rearrangement in the pore.

 In conclusion, even if the (de)hydration effect has been mostly ignored, our results clearly

show its impact on the properties of the adsorbed hhMb. Further studies are required to fully

understand this phenomenon and different mesoporous substrate and proteins have to be

investigated to asses to which extent the effect is depending on the type of host material and

biomolecule.

This paper clearly proves that the effect of both (de)hydration and confinement has to be

considered for the future applicability of the immobilized biomolecule, since they affect

activity and structure of the biomolecule.

Supporting Information

Surface characterization of MT8 and MT17

Langmuir model isotherms for the adsorption of hhMb in MT17 and MT8.

Mass kinematograms relative to the thermal decomposition of hhMb in hhMb-MT8_15, hhMb-MT8_120, hhMb-MT17_15 and hhMb-MT17_120, DTG profiles of MT8 and MT17, UV-vis DR spectra of lyophilized hhMb, hhMb-MT8_15, hhMb-MT8_120, hhMb-MT17_15 and hhMb-MT17_120. Low-field area of the normalized CW-EPR spectra. Protein structure. Normalized EPR spectra and simulations.

References

(1)   Fried, D. I.; Brieler, F. J.; Fröba, M. Designing Inorganic Porous Materials for Enzyme Adsorption and Applications in Biocatalysis. *ChemCatChem* **2013**, *5*, 862–884.

(2)   Kim, J.; Grate, J. W.; Wang, P. Nanostructures for Enzyme Stabilization. *Chem. Eng. Sci.* **2006**, *61*, 1017–1026.

(3)   Davis, M. E. Ordered Porous Materials for Emerging Applications. *Nature* **2002**, *417*, 813–821.

(4)   Eggers, D. K.; Valentine, J. S. Crowding and Hydration Effects on Protein Conformation: A Study with Sol-Gel Encapsulated Proteins. *J. Mol. Biol.* **2001**, *314*, 911–922.

(5)   Eggers, D. K.; Valentine, J. S. Molecular Confinement Influences Protein Structure and Enhances Thermal Protein Stability. *Protein Sci.* **2001**, *10*, 250–261.

(6)   Hudson, S.; Cooney, J.; Magner, E. Proteins in Mesoporous Silicates. *Angew. Chem. Int. Ed. Engl.* **2008**, *47*, 8582–8594.

(7)   Miyahara, M.; Vinu, A.; Ariga, K. Adsorption Myoglobin over Mesoporous Silica Molecular Sieves: Pore Size Effect and Pore-Filling Model. *Mater. Sci. Eng. C* **2007**, *27*, 232–236.

(8)   Magner, E. Immobilisation of Enzymes on Mesoporous Silicate Materials. *Chem. Soc. Rev.* **2013**, *42*, 6213–6222.

(9)   Minton, A. P. Confinement as a Determinant of Macromolecular Structure and Reactivity. *Biophys. J.* **1992**, *63*, 1090–1100.

(10)   Santos, J. C. S. D.; Barbosa, O.; Ortiz, C.; Berenguer-Murcia, A.; Rodrigues, R. C.; Fernandez-Lafuente, R. Importance of the Support Properties for Immobilization or Purification of Enzymes. *ChemCatChem* **2015**, *7*, 2413–2432.

1 (11) Essa, H.; Magner, E.; Cooney, J.; Hodnett, B. K. Influence of PH and Ionic Strength on the Adsorption,

2   Leaching and Activity of Myoglobin Immobilized onto Ordered Mesoporous Silicates. *J. Mol. Catal. B*

3   *Enzym.* **2007**, *49*, 61–68.

4 (12) Itoh, T.; Ishii, R.; Ebina, T.; Hanaoka, T.; Fukushima, Y.; Mizukami, F. Encapsulation of Myoglobin with a

5   Mesoporous Silicate Results in New Capabilities. *Bioconjug. Chem.* **2006**, *17*, 236–240.

6 (13) Lynch, M. M.; Liu, J.; Nigra, M.; Coppens, M. O. Chaperonin-Inspired PH Protection by Mesoporous

7   Silica SBA-15 on Myoglobin and Lysozyme. *Langmuir* **2016**, *32* (37), 9604–9610.

8 (14) Takimoto, A.; Shiomi, T.; Ino, K.; Tsunoda, T.; Kawai, A.; Mizukami, F.; Sakaguchi, K. Encapsulation of

9   Cellulase with Mesoporous Silica (SBA-15). *Microporous Mesoporous Mater.* **2008**, *116*, 601–606.

10 (15) Penna, M. J.; Mijajlovic, M.; Biggs, M. J. Molecular-Level Understanding of Protein Adsorption at the

11   Interface between Water and a Strongly-Interacting Uncharged Solid Surface. *J. Am. Chem. Soc.* **2014**,

12   *136*, 5323–5331.

13 (16) Schirò, G.; Sclafani, M.; Natali, F.; Cupane, A. Hydration Dependent Dynamics in Sol-Gel Encapsulated

14   Myoglobin. *Eur. Biophys. J.* **2008**, *37*, 543–549.

15 (17) Jamadagni, S. N.; Godawat, R.; Dordick, J. S.; Garde, S. How Interfaces Affect Hydrophobically Driven

16   Polymer Folding. *J. Phys. Chem. B* **2009**, *113*, 4093–4101.

17 (18) Pocker, Y. Water in Enzyme Reactions: Biophysical Aspects of Hydration-Dehydration Processes. *Cell.*

18   *Mol. Life Sci.* **2000**, *57*, 1008–1017.

19 (19) Zhang, S. Hydrogels: Wet or Let Die. *Nat. Mater.* **2004**, *3*, 7–8.

20 (20) Gupta, R.; Chaudhury, N. K. Entrapment of Biomolecules in Sol-Gel Matrix for Applications in

21   Biosensors: Problems and Future Prospects. *Biosens. Bioelectron.* **2007**, *22*, 2387–2399.

22 (21) Ravindra, R.; Zhao, S.; Gies, H.; Winter, R. Protein Encapsulation in Mesoporous Silicate: The Effects of

23   Confinement on Protein Stability, Hydration, and Volumetric Properties. *J. Am. Chem. Soc.* **2004**, *126*,

24   12224–12225.

25 (22) Adiram-Filiba, N.; Schremer, A.; Ohaion, E.; Nadav-Tsubery, M.; Lublin-Tennenbaum, T.; Keinan-

26   Adamsky, K.; Goobes, G. Ubiquitin Immobilized on Mesoporous MCM41 Silica Surfaces – Analysis by

1 Solid-State NMR with Biophysical and Surface Characterization. *Biointerphases* **2017**, *12*, 02D414/1-9.

2 (23) Ikemoto, H.; Tubasum, S.; Pullerits, T.; Ulstrup, J.; Chi, Q. Nanoscale Confinement and Fluorescence

3   Effects of Bacterial Light Harvesting Complex LH2 in Mesoporous Silicas. *J. Phys. Chem. C* **2013**, *117*,

4   2868–2878.

5 (24) Zhu, Y.; Ren, T.; Yuan, Z. Mesoporous Non-Siliceous Inorganic–organic Hybrids: A Promising Platform for

6   Designing Multifunctional Materials. *New J. Chem.* **2014**, *38*, 1905–1922.

7 (25) Jia, N.; Wen, Y.; Yang, G.; Lian, Q.; Xu, C.; Shen, H. Direct Electrochemistry and Enzymatic Activity of

8   Hemoglobin Immobilized in Ordered Mesoporous Titanium Oxide Matrix. *Electrochem. commun.* **2008**,

9   *10*, 774–777.

10 (26) Rahemi, V.; Trashin, S.; Meynen, V.; De Wael, K. An Adhesive Conducting Electrode Material Based on

11   Commercial Mesoporous Titanium Dioxide as a Support for Horseradish Peroxidase for

12   Bioelectrochemical Applications. *Talanta* **2016**, *146*, 689–693.

13 (27) Wehmeyer, J. L.; Synowicki, R.; Bizios, R.; Garcia, C. D. Dynamic Adsorption of Albumin on

14   Nanostructured TiO2 Thin Films. *Mater. Sci. Eng. C* **2010**, *30*, 277–282.

15 (28) Popat, K. C.; Eltgroth, M.; LaTempa, T. J.; Grimes, C. A.; Desai, T. A. Titania Nanotubes: A Novel Platform

16   for Drug-Eluting Coatings for Medical Implants? *Small* **2007**, *3*, 1878–1881.

17 (29) Liu, A.; Wei, M.; Honma, I.; Zhou, H. Direct Electrochemistry of Myoglobin in Titanate Nanotubes Film.

18   *Anal. Chem.* **2005**, *77*, 8068–8074.

19 (30) Bai, Y.; Angelis, F. D.; Bisquert, J.; Wang, P. Titanium Dioxide Nanomaterials for Sensor Applications.

20   *Chem. Rev.* **2014**, *114*, 10131–10176.

21 (31) Hou, J.; Dong, G.; Ye, Y.; Chen, V. Laccase Immobilization on Titania Nanoparticles and Titania-

22   Functionalized Membranes. *J. Memb. Sci.* **2014**, *452*, 229–240.

23 (32) Vivero-Escoto, J. L.; Chiang, Y.-D.; Wu, K. C.-W.; Yamauchi, Y. Recent Progress in Mesoporous Titania

24   Materials: Adjusting Morphology for Innovative Applications. *Sci. Technol. Adv. Mater.* **2012**, *13*, 1–9.

25 (33) Rajh, T.; Dimitrijevic, N. M.; Bissonnette, M.; Koritarov, T.; Konda, V. Titanium Dioxide in the Service of

26   the Biomedical Revolution. *Chem. Rev.* **2014**, *114*, 10177–10216.

1   (34)   Karlsson, J.; Atefyekta, S.; Andersson, M. Controlling Drug Delivery Kinetics from Mesoporous Titania
2   Thin Films by Pore Size and Surface Energy. *Int. J. Nanomedicine* **2015**, *10*, 4425–4436.

3   (35)   Loreto, S.; Vanrompay, H.; Mertens, M.; Bals, S.; Meynen, V. The Influence of Acids on Tuning the Pore
4   Size of Mesoporous TiO2 Templated by Non-Ionic Block Copolymers. *Eur. J. Inorg. Chem.* **2018**, *2018*,
5   62–65.

6   (36)   Chaudhary, Y. S.; Manna, S. K.; Mazumdar, S.; Khushalani, D. Protein Encapsulation into Mesoporous
7   Silica Hosts. *Microporous Mesoporous Mater.* **2008**, *109*, 535–541.

8   (37)   Evans, S. V; Brayert, G. D. High-Resolution Study of the Three-Dimensional Structure of Horse Heart
9   Metmyoglobin. *J. Mol. Biol.* **1990**, *213*, 885–897.

10 (38)   Loreto, S.; Cuypers, B.; Brokken, J.; Van Doorslaer, S.; De Wael, K.; Meynen, V. The Effect of Buffer
11   Solution on the Adsorption and Stability of Horse Heart Myoglobin in Commercial Mesoporous
12   Titanium Dioxide : A Matter of the Right Choice . *Phys. Chem. Chem. Phys.* **2017**, *19*, 13503–13514.

13 (39)   Kadnikova, E. N.; Kostić, N. M. Oxidation of ABTS by Hydrogen Peroxide Catalyzed by Horseradish
14   Peroxidase Encapsulated into Sol-Gel Glass. Effects of Glass Matrix on Reactivity. *J. Mol. Catal. B Enzym.*
15   **2002**, *18*, 39–48.

16 (40)   Yang, H.; Yang, S.; Kong, J.; Dong, A.; Yu, S. Obtaining Information about Protein Secondary Structures in
17   Aqueous Solution Using Fourier Transform IR Spectroscopy. *Nat. Protoc.* **2015**, *10*, 382–396.

18 (41)   Stoll, S.; Schweiger, A. EasySpin, a Comprehensive Software Package for Spectral Simulation and
19   Analysis in EPR. *J. Magn. Reson.* **2006**, *178*, 42–55.

20 (42)   Michel, R.; Pasche, S.; Textor, M.; Castenr, D. G. The Influence of PEG Architecture on Protein
21   Adsorption and Conformation. *Langmuir* **2005**, *21* (3), 12327–12332.

22 (43)   Roach, P.; Farrar, D.; Perry, C. C. Interpretation of Protein Adsorption: Surface-Induced Conformational
23   Changes. *J. Am. Chem. Soc.* **2005**, *127*, 8168–8173.

24 (44)   Kijima, J.; Shibuya, Y.; Katayama, K.; Itoh, T.; Iwase, H.; Fukushima, Y.; Kubo, M.; Yamaguchi, A.
25   Structural Characterization of Myoglobin Molecules Adsorbed within Mesoporous Silicas. *J. Phys. Chem.*
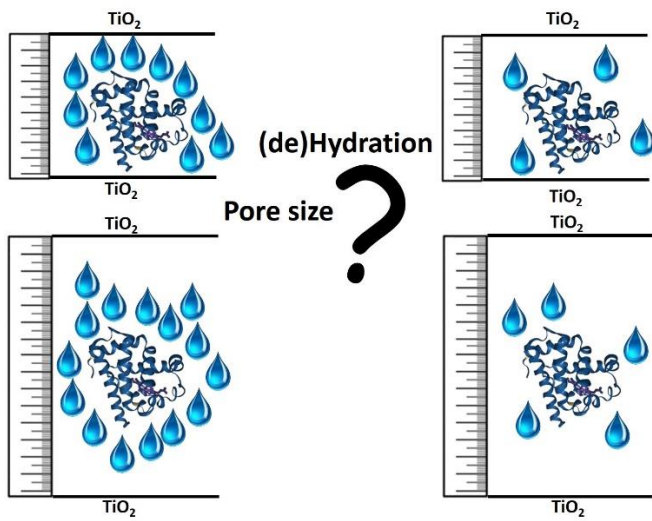26   *C* **2018**, *122*, 15567–15574.

1   (45)   Takeuchi, M.; Bertinetti, L.; Martra, G.; Coluccia, S.; Anpo, M. States of H2O Adsorbed on Oxides: An

2   Investigation by near and Mid Infrared Spectroscopy. *Appl. Catal. A Gen.* **2006**, *307* (1), 13–20.

3   (46)   Martra, G. Lewis Acid and Base Sites at the Surface of Microcrystalline TiO2 Anatase: Relationships

4   between Surface Morphology and Chemical Behaviour. *Appl. Catal. A Gen.* **2000**, *200*, 275–285.

5   (47)   Morterra, C. An Infrared Study of Anatase Properties. *J. Chem. Soc. Faraday Transit. 1* **1988**, *84*, 1617–

6   1637.

7   (48)   Gray, J. J. The Interaction of Proteins with Solid Surfaces. *Curr. Opin. Struct. Biol.* **2004**, *14* (1), 110–115.

8   (49)   Weber, E.; Sirim, D.; Schreiber, T.; Thomas, B.; Pleiss, J.; Hunger, M.; Gläser, R.; Urlacher, V. B.

9   Immobilization of P450 BM-3 Monooxygenase on Mesoporous Molecular Sieves with Different Pore

10   Diameters. *J. Mol. Catal. B Enzym.* **2010**, *64*, 29–37.

11   (50)   Vinu, A.; Gokulakrishnan, N.; Balasubramanian, V. V.; Alam, S.; Kapoor, M. P.; Ariga, K.; Mori, T. Three-

12   Dimensional Ultralarge-Pore Ia3d Mesoporous Silica with Various Pore Diameters and Their Application

13   in Biomolecule Immobilization. *Chem. - A Eur. J.* **2008**, *14*, 11529–11538.

14   (51)   Chalikian, T. V.; Totrov, M.; Abagyan, R.; Breslauer, K. J. The Hydration of Globular Proteins as Derived

15   from Volume and Compressibility Measurements: Cross Correlating Thermodynamic and Structural

16   Data. *J. Mol. Biol.* **1996**, *260*, 588–603.

17   (52)   Deere, J.; Magner, E.; Wall, J. G.; Hodnett, B. K. Mechanistic and Structural Features of Protein

18   Adsorption onto Mesoporous Silicates. *J. Phys. Chem. B* **2002**, *106*, 7340–7347.

19   (53)   Latour, R. A. The Langmuir Isotherm: A Commonly Applied but Misleading Approach for the Analysis of

20   Protein Adsorption Behavior. *J. Biomed. Mater. Res. - Part A* **2015**, *103*, 949–958.

21   (54)   Barth, A. Infrared Spectroscopy of Proteins. *Biochim. Biophys. Acta* **2007**, *1767*, 1073–1101.

22   (55)   Si, P.; Ding, S.; Yuan, J.; Lou, X. W.; Kim, D. H. Hierarchically Structured One-Dimensional TiO2 for

23   Protein Immobilization, Direct Electrochemistry, and Mediator-Free Glucose Sensing. *ACS Nano* **2011**, *5*,

24   7617–7626.

25   (56)   Liu, C.; Guo, Y.; Hong, Q.; Rao, C.; Zhang, H.; Dong, Y.; Huang, L.; Lu, X.; Bao, N. Bovine Serum Albumin

26   Adsorption in Mesoporous Titanium Dioxide: Pore Size and Pore Chemistry Effect. *Langmuir* **2016**, *32*,

1 3995–4003.

2 (57) Meersman, F.; Smeller, L.; Heremans, K. Comparative Fourier Transform Infrared Spectroscopy Study of

3 Cold-, Pressure-, and Heat-Induced Unfolding and Aggregation of Myoglobin. *Biophys. J.* **2002**, *82*,

4 2635–2644.

5 (58) Zhou, Z.; Inayat, A.; Schwieger, W.; Hartmann, M. Improved Activity and Stability of Lipase Immobilized

6 in Cage-like Large Pore Mesoporous Organosilicas. *Microporous Mesoporous Mater.* **2012**, *154*, 133–

7 141.

8 (59) Jiang, X.; Jiang, J.; Jin, Y.; Wang, E.; Dong, S. Effect of Colloidal Gold Size on the Conformational Changes

9 of Adsorbed Cytochrome c: Probing by Circular Dichroism, UV-Visible, and Infrared Spectroscopy.

10 *Biomacromolecules* **2005**, *6*, 46–53.

11 (60) Sang, L.-C.; Coppens, M.-O. Effects of Surface Curvature and Surface Chemistry on the Structure and

12 Activity of Proteins Adsorbed in Nanopores. *Phys. Chem. Chem. Phys.* **2011**, *13*, 6689–6698.

13 (61) Dong, A.; Huang, P.; Caughey, W. S. Protein Secondary Structures in Water from Second-Derivative

14 Amide I Infrared Spectra. *Biochemistry* **1990**, *29*, 3303–3308.

15 (62) Evans, S. V; Brayer, G. D. Horse Heart Metmyoglobin. *J. Biol. Chem.* **1988**, *263*, 4263–4268.

16 (63) Norde, W. Adsorption of Proteins from Solution at the Solid-Liquid Interface. *Adv. Colloid Interface Sci.*

17 **1986**, *25*, 267–340.

18 (64) Yu, L.; Zhang, L.; Sun, Y. Protein Behavior at Surfaces: Orientation, Conformational Transitions and

19 Transport. *J. Chromatogr. A* **2015**, *1382*, 118–134.

20 (65) Devineau, S.; Zargarian, L.; Renault, J. P.; Pin, S. Structure and Function of Adsorbed Hemoglobin on

21 Silica Nanoparticles: Relationship between the Adsorption Process and the Oxygen Binding Properties.

22 *Langmuir* **2017**, *33*, 3241–3252.

23 (66) Menaa, B.; Miyagawa, Y.; Takahashi, M.; Herrero, M.; Rives, V.; Menaa, F.; Eggers, D. K.

24 Bioencapsulation of Apomyoglobin in Nanoporous Organosilica Sol-Gel Glasses: Influence of the

25 Siloxane Network on the Conformation and Stability of a Model Protein. *Biopolymers* **2009**, *91*, 895–

26 906.

1   (67)   Griebenow, K.; Klibanov, A. M. Lyophilization-Induced Reversible Changes in the Secondary Structure of

2   Proteins. *Proc. Natl. Acad. Sci. U. S. A.* **1995**, *92*, 10969–10976.

3   (68)   Prestrelski, S. J.; Tedeschi, N.; Arakawa, T.; Carpenter, J. F. Dehydration-Induced Conformational

4   Transitions in Proteins and Their Inhibition by Stabilizers. *Biophys. J.* **1993**, *65*, 661–671.

5   (69)   Privalov, P. L. Thermodynamic Bases of the Stability of Protein Structure. *Thermochim. Acta* **1990**, *163*,

6   33–46.

7   (70)   Snyder, A. P.; Tripathi, A.; Dworzanski, J. P.; Maswadeh, W. M.; Wick, C. H. Characterization of

8   Microorganisms by Thermogravimetric Analysis–mass Spectrometry. *Anal. Chim. Acta* **2005**, *536*, 283–

9   293.

10   (71)   Jiang, X.; Smith, J.; Abraham, E. Identification of a MS-MS Fragment Iagnostic for Methionine Sulfoxide.

11   *J. Mass Spectrom. Lett.* **1996**, *31*, 1309–1310.

12   (72)   Schmidt, V.; Giacomelli, C.; Soldi, V. Thermal Stability of Films Formed by Soy Protein Isolate–sodium

13   Dodecyl Sulfate. *Polym. Degrad. Stab.* **2005**, *87*, 25–31.

14   (73)   Mallamace, F.; Corsaro, C.; Mallamace, D.; Vasi, S.; Vasi, C.; Baglioni, P.; Buldyrev, S. V.; Chen, S.-H.;

15   Stanley, H. E. Energy Landscape in Protein Folding and Unfolding. *Proc. Natl. Acad. Sci.* **2016**, *113*,

16   3159–3163.

17   (74)   Rathore, N.; Knotts IV, T. A.; De Pablo, J. J. Confinement Effects on the Thermodynamics of Protein

18   Folding: Monte Carlo Simulations. *Biophys. J.* **2006**, *90*, 1767–1773.

19   (75)   Anderson, A. B.; Robertson, C. R. Absorption Spectra Indicate Conformational Alteration of Myoglobin

20   Adsorbed on Polydimethylsiloxane. *Biophys. J.* **1995**, *68*, 2091–2097.

21   (76)   Chi, Z.; Asher, S. A. UV Resonance Raman Determination of Protein Acid Denaturation: Selective

22   Unfolding of Helical Segments of Horse Myoglobin. *Biochemistry* **1998**, *37*, 2865–2872.

23   (77)   Scholes, C. P.; Isaacson, R. A.; Feher, G. Determination of the Zero-Field Splitting of Fe3+ in Heme

24   Proteins from the Temperature Dependance of the Spin-Lattice Relaxation Rate. *Biochim. Biophys. Acta*

25   **1971**, *244*, 206–210.

26   (78)   Xiong, L. Bin; Li, J. L.; Yang, B.; Yu, Y. Ti 3+ in the Surface of Titanium Dioxide: Generation, Properties

and Photocatalytic Application. *J. Nanomater.* **2012**, *2012*, 1–13.

(79)   Han, Y. J.; Watson, J. T.; Stucky, G. D.; Butler, A. Catalytic Activity of Mesoporous Silicate-Immobilized

Chloroperoxidase. *J. Mol. Catal. - B Enzym.* **2002**, *17* (1), 1–8.

(80)   Ramírez-Montoya, L. A.; Concheso, A.; Alonso-Buenaposada, I. D.; García, H.; Angel Menéndez, J.;

Arenillas, A.; Montes-Morán, M. A. Protein Adsorption and Activity on Carbon Xerogels with Narrow

Pore Size Distributions Covering a Wide Mesoporous Range. *Carbon N. Y.* **2017**, *118*, 743–751.

(81)   Takahashi, H.; Li, B.; Sasaki, T.; Miyazaki, C.; Kajino, T.; Inagaki, S. Catalytic Activity in Organic Solvents

and Stability of Immobilized Enzymes Depend on the Pore Size and Surface Characteristics of

Mesoporous Silica. *Chem. Mater.* **2000**, *12*, 3301–3305.

(82)   El-boubbou, K.; Scho, D. A.; Landry, C. C. Enhanced Enzymatic Activity of OPH in Ammonium-

Functionalized Mesoporous Silica: Surface Modification and Pore Effects. *J. Phys. Chem. C* **2012**, *116*,

17501–17506.

(83)   Frenkel-Mullerad, H.; Avnir, D. Sol-Gel Materials as Efficient Enzyme Protectors: Preserving the Activity

of Phosphatases under Extreme PH Conditions. *J. Am. Chem. Soc.* **2005**, *127*, 8077–8081.

TOC graphic